Electronic Supplementary Information

Salt-assisted pyrolysis of carbon nanosheets and carbon nanoparticles hybrids for efficient microwave absorption

Wenjian Wang†[a], Weiping Ye†[a], Xingwang Hou[a],Ke Ran[a], Yilin Huang[a], Zidong Zhang[a], Yuan Fang[a], Shuai Wang[a], Rui Zhao*[a] and Weidong Xue*[a]

[a]School of Materials and Energy, University of Electronic Science and Technology of China, Chengdu 610054, PR China.

†Wenjian Wang and Weiping Ye made equal contributions to this work (Co-first authors).

*Corresponding authors

E-mail addresses: ruizhao@uestc.edu.cn (R. Zhao), xuewd@uestc.edu.cn (WD. Xue)

Contents

1. Experimental details

1.1 Materials and methods

2.89g $Zn(NO_3)_2$·6H2O and 3.29g 2-methylimidazole were dissolved in 60 ml methanol by stirring for 15 min, respectively. Then the 2-MIM methanol solution was quickly poured into the $Zn(NO_3)_2$·6H2O methanol solution, stirred at room temperature for 2h, and then left to rest for 2h. The ZIF-8 precipitate was then collected by centrifugation, washed three times with methanol, followed dried in an oven at 60 ºC overnight.

0.3 g ZIF-8 powder and 6 g KCl were physically mixed by grinding for 10 min, after which the mixture was placed in a quartz tube, heated at 900 ºC under Ar flow for 2h. The product was washed with deionized water to remove KCl. Finally, the N-doped carbon (denoted as NC-KCl) was dried under vacuum at 70 ºC for 24h.

To investigate the effect of the different types of salt on the properties and performance of the carbon sheets, several further N-doped carbon sheets were prepared by replacing NaCl with KCl or mixed salt (n_{NaCl}: n_{KCl} = 1:1), which are denoted herein as NC-KCl and NC-NaCl/KCl, respectively. As a comparison, the ZIF-8 powder was annealed directly in an argon atmosphere for 2h and the obtained product was named NC.

1.2 Characterization

The structure and morphology were characterized via the scanning electron microscope (SEM, Phenom ProX) and transmission electron microscopy (TEM, JEM-2100F). X-ray diffraction (XRD) patterns were obtained on the Dandong Haoyuan diffractometer (DX-27mini). Raman spectra were obtained on HORIBA. The specific surface areas and pore size distribution were calculated from the results of N_2 physisorption at 77 K on two kinds of equipment (mesoporous on TriStar II 3020 and all

the hole on ASAP 2460). X-ray photoelectron spectroscopy (XPS) analyses were carried out with Thermo Scientific. The electromagnetic parameters of the samples were measured by a vector network analyzer (Keysight E5063A) in the frequency range of 2-18 GHz with the coaxial wire method. The sample material powder and the paraffin block were mixed in a ratio of 7:93 and heated. The mixture was sharpened into cylindrical rings with an inner diameter of 3.04 mm and an outer diameter of 7.0 mm using a mold.

2. Simulation of the monostatic radar cross section (RCS)

Computer Simulation Techniques Microwave Studio (CST MWS) software investigates the response of absorbers to specific frequency electromagnetic waves through integral equation solver. According to the single-layer homogeneous absorber model, a simulation model of the specimen was built as a square (30 × 30 cm2) with two layers, consisting of an absorber layer with the thickness of 1.7 mm and a backing plate of perfect electric conductor (PEC), with the thickness of 4 mm. The measured electromagnetic parameters are imported into CST, and the electromagnetic parameters of the absorber are obtained by fitting with the dispersion model. Open (add space) boundary conditions are set in all directions. The field monitor frequency is set to 17.04 GHz, and the monitor type is RCS. The linear polarized plane wave is used, and the electric polarization propagation direction is along the X-axis. The RCS values can be calculated according to the following equation:

$$\sigma\left(dBm^2\right) = 10log\left[\frac{4\pi S}{\lambda^2}\left|\frac{E_S}{E_i}\right|^2\right]\#(1)$$

here, S is the area of the target object simulation model, λ is the wave length of electromagnetic wave, E_s is the electric field intensity of transmitting waves, and E_i is the electric field intensity of receiving waves.

3. Numerical Simulation

Numerical models were developed in COMSOL software to study the electromagnetic wave energy loss mechanism of the samples. Two corresponding simulation models were established in order to investigate the difference in electromagnetic energy loss capacity of isolated carbon nanoparticles and 3D carbon networks. Incident microwaves with an excitation power of 1 w (frequencies of 14 GHz) from the source are injected into the MA material along the z-axis (x-axis in the direction of electric field polarization and y-axis in the direction of magnetic field polarization). Exactly matched layers are used at the top and bottom of the computational domain to absorb the reflected and transmitted microwaves, respectively. The electromagnetic field in the simulation domain is obtained by solving Maxwell's set of equations in the frequency domain. The specific material parameters for simulation are listed below:

Materials	ε	tanε	σ/(S·m^{-1})
Epoxy	2.7	0.02	0
Carbon C	1	0	400

4. The Debye models

$$\left(\varepsilon' - \frac{\varepsilon_s + \varepsilon_\infty}{2}\right)^2 + \left(\varepsilon''\right)^2 = \left(\frac{\varepsilon_s - \varepsilon_\infty}{2}\right)^2 \#(S1)$$

where ε_s and ε_∞ represent static permittivity and high-frequency limit permittivity.

5. Attenuation coefficient (α)

The attenuation coefficient (α) can be expressed by the following equation[1]:

$$\alpha = \frac{\sqrt{2}\pi f}{c}\sqrt{\left(\mu''\varepsilon'' - \mu'\varepsilon'\right) + \sqrt{\left(\mu''\varepsilon'' - \mu'\varepsilon'\right)^2 + \left(\mu'\varepsilon'' + \mu''\varepsilon'\right)^2}} \#(S2)$$

Where μ', μ'' and ε', ε'' represent the real part and imaginary part of complex permeability and complex permittivity respectively, f refers to the frequency of the electromagnetic wave. Meanwhile, c is a proxy

for the velocity of light propagation in a vacuum.

6. The reflection loss (RL) and effective absorption bandwidth (EAB)

Based on transmission line theory, the RL with different thicknesses can be calculated by the following equation[2]:

$$RL(dB) = 20lg\left|\frac{Z_{in} - Z_0}{Z_{in} + Z_0}\right| \#(S3)$$

Herein, Z_0 represents the impedance of air, and Z_{in} is the input impedance of materials, which can be expressed by the formulae:

$$Z_{in} = Z_0\sqrt{\frac{\mu_r}{\varepsilon_r}}\tanh\left[j\left(\frac{2\pi f d}{c}\right)\sqrt{\mu_r\varepsilon_r}\right] \#(S4)$$

Where μ_r and ε_r represent the complex permeability and complex permittivity respectively, f and d refer to the frequency of the electromagnetic wave and the thickness of the absorber respectively, and c is a constant proxy for the velocity of light propagation in a vacuum. Generally speaking, RL < -10dB, i.e. 90% attenuation of electromagnetic energy, is considered the criterion for effective absorption.

7. 1/4 Wavelength Theory

$$t_m = \frac{n\lambda}{4} = \frac{nc}{4f_m\sqrt{|\varepsilon_r||\mu_r|}}(n = 1, 3, 5, \ldots) \#(S5)$$

where t_m is the matched thickness, λ is the electromagnetic wave wavelength, c is the velocity of light, and f_m is the matched frequency.

8. Figure and Table

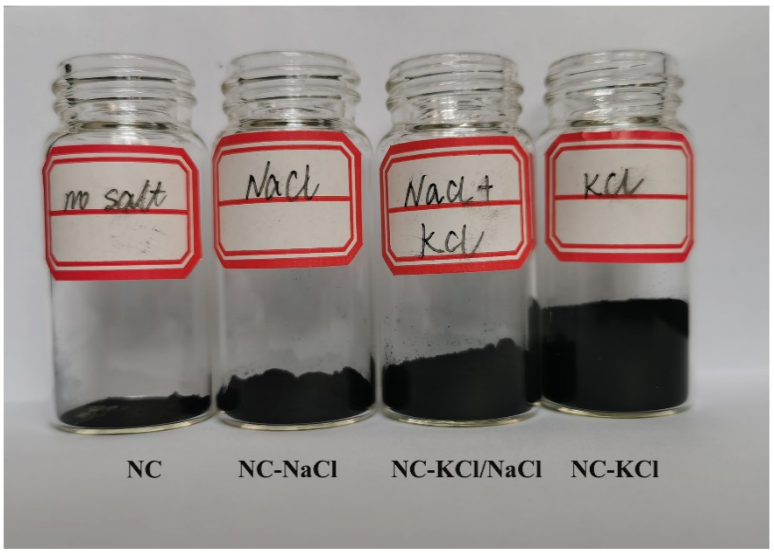

Figure S1. Optical photos of all products.

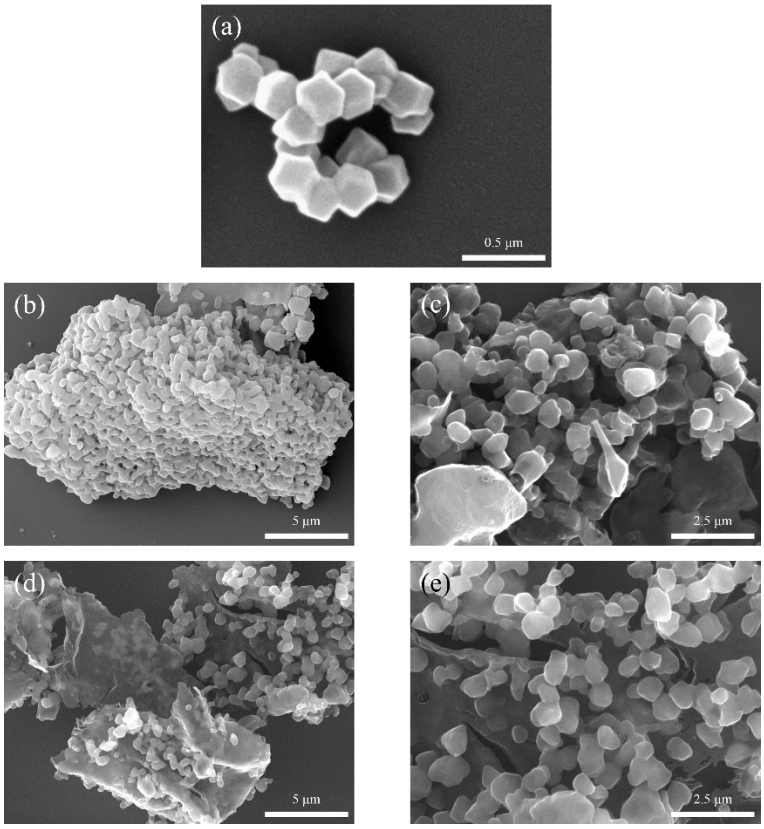

Figure S2. SEM image of (a)ZIF-8, (b, c) NC-KCl/NaCl and (d, e) NC-NaCl sample.

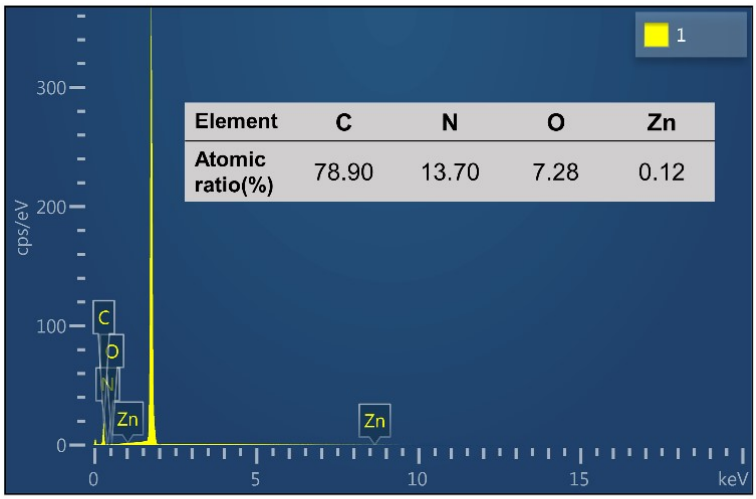

Figure S3. EDS of NC-KCl sample.

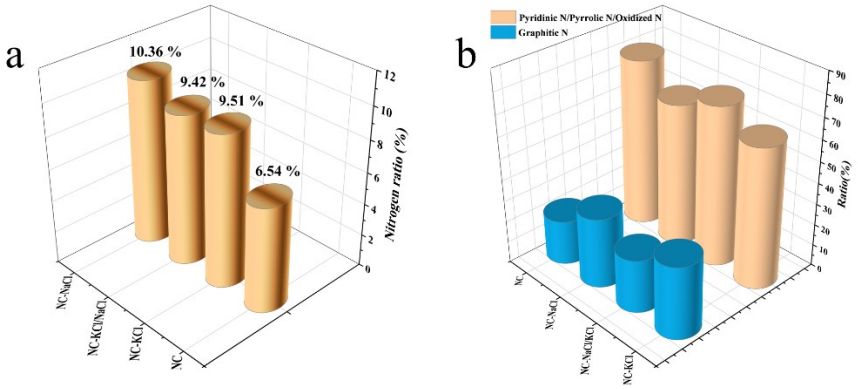

Figure S4. (a) Nitrogen ratio and (b) elemental nitrogen species for all samples.

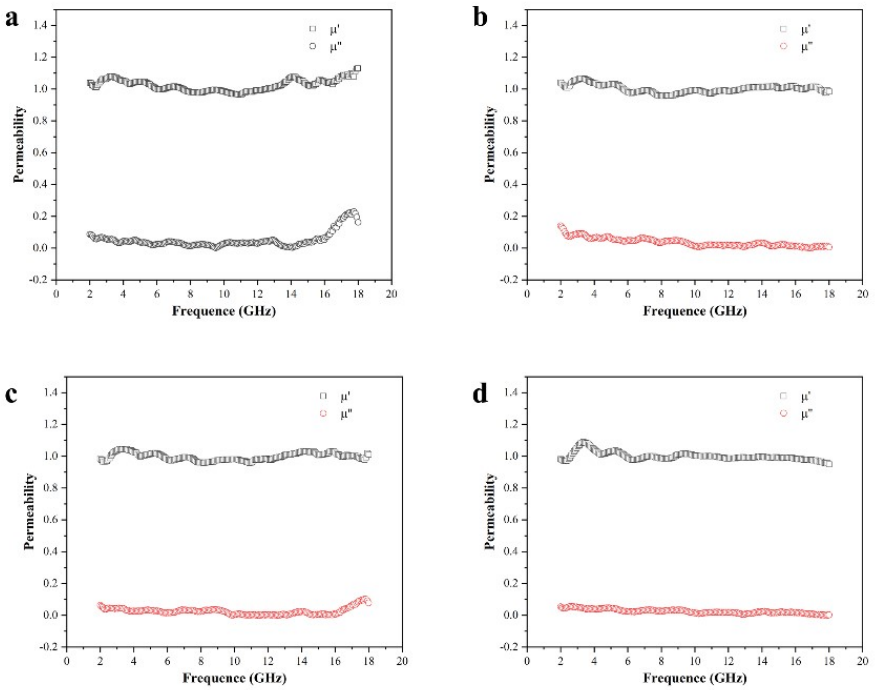

Figure S5. Complex permeability of all samples. (a) NC-KCl, (b) NC-KCl/NaCl, (c) NC- NaCl, (d) NC

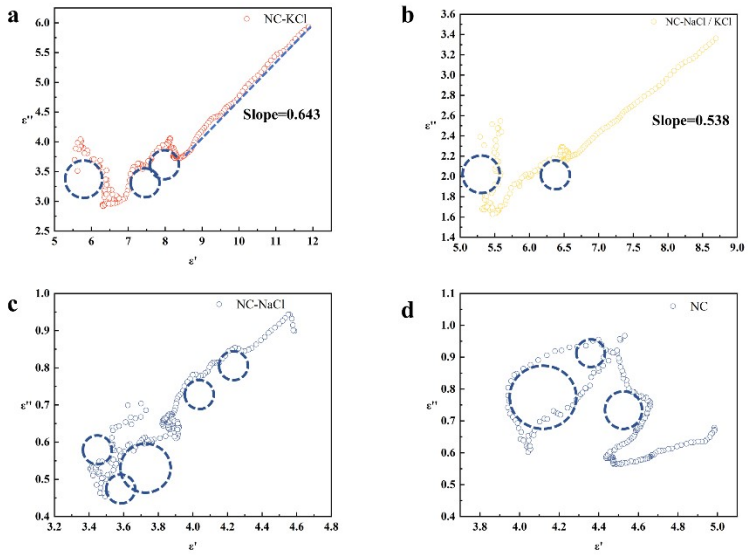

Figure S6. Cole–Cole curves of all samples.

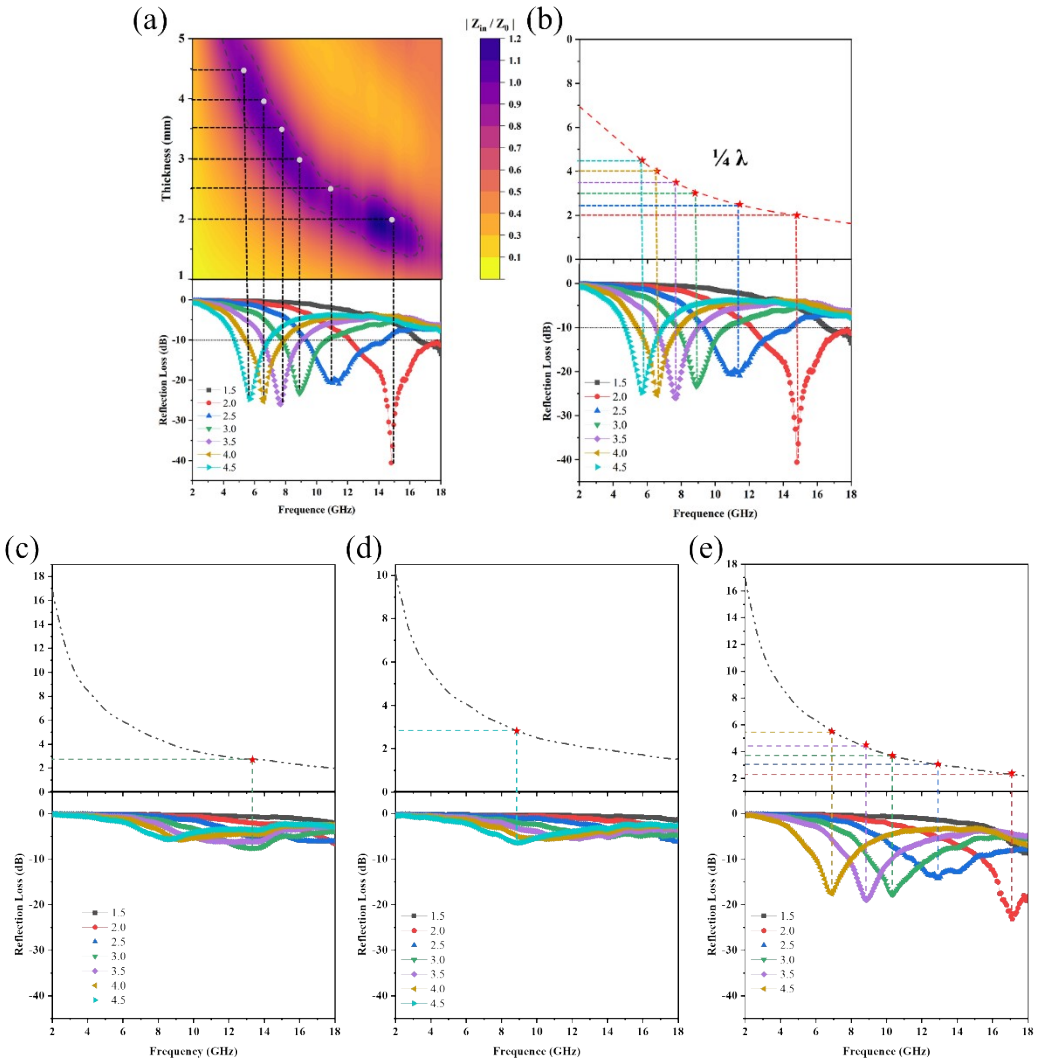

Figure S7. Curves of (a) NC-KCl versus normalized impedance and

curves of λ/4 (b) NC-KCl (c)NC, (d)NC-NaCl, (e) NC-KCl/NaCl

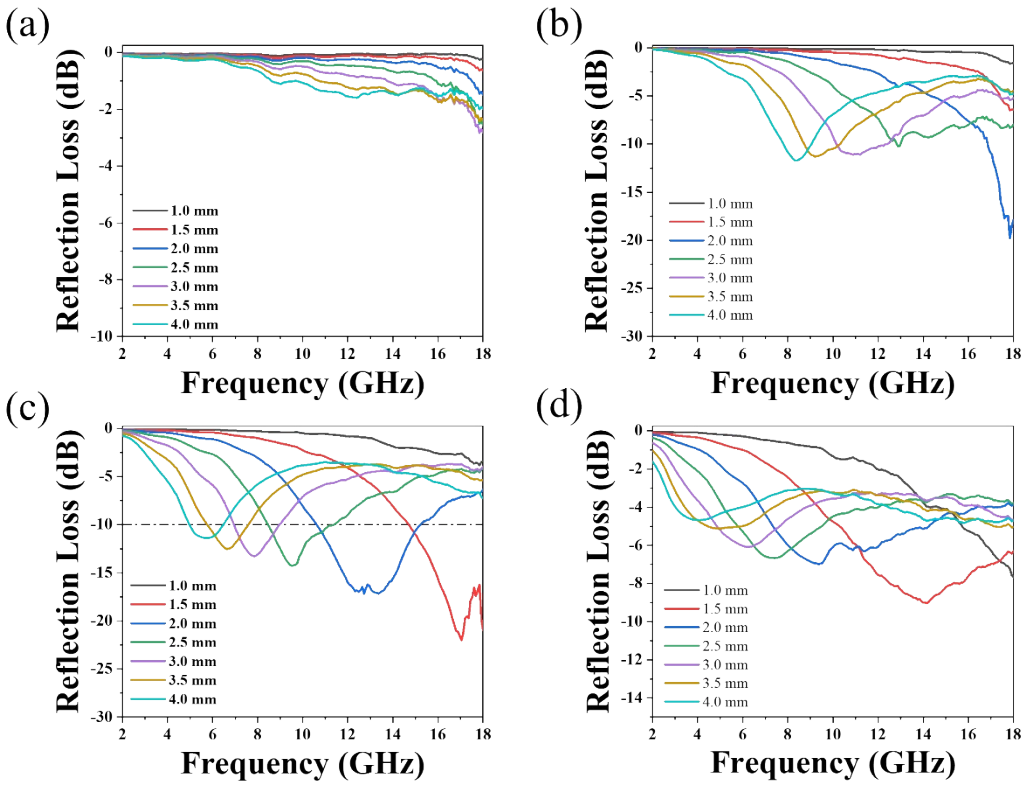

Figure S8. 2D representations of reflection loss of (a)1%, (b)5%, (c)10%, (d)15% of NC-KCl composite in paraffin matrix.

Table S1. A summary comparison of microwave absorption properties of representative MOF derived carbon-based composites in recent literatures.

MAMs	MOFs	Ratio (wt%)
ZrO_2/C	UIO-66	50
Co@NCNT-octahedron	ZIF-67-octahedron	25
$Ni_{1-x}Co_x$@C	Ni-Co-MOF	25
Ni@C@ZnO	NiZn-MOF	25
Co_3ZnC-Co@N/C	$ZnCo_2O_4$@ZIF-67	30
CoFe alloys@ZnO@	Fe_2O_3@ZnCo-MOF	30
N-Ni-Co_xS_y/Ni_xS_y@	Ni-ZIF67/S@C	25
CF@C/Co	CF@ZIF-67	20
NC-KCl	ZIF-8	7

Refs.	d (mm) corresponding to EAB	EAB (GHz)	d (mm) corresponding to RL_{min}	*f* (GHz) corresponding to RL_{min}	RL_{min} (dB)
[3]	1.7	5.5	1.5	16.8	-58.7
[4]	2	6.2	1.8	16.8	-53
[5]	2.2	4.9	4.5	6	-59.5
[6]	—	4.1	2.5	—	-55.8
[7]	1.97	5.23	4.22	5.6	-67.97
[8]	5.84	5.84	5	—	-44.13
[9]	1.5	3.95	2	11.7	-48.3
[10]	1.71	6.25	1.78	—	-71.95
This	2.1	6.24	2	14.8	-40.58

9. Reference:

1 W. Yang, Q. Zhao, Y. Zhou, Z. Cui and Y. Liu, *Adv. Eng. Mater.*, 2021, 2100964.

2 Y. Fang, W. Xue, R. Zhao, S. Bao, W. Wang, L. Sun, L. Chen, G. Sun and B. Chen, *J. Mater. Chem. C*, 2019, **8**, 319–327.

3 X. Zhang, J. Qiao, C. Liu, F. Wang, Y. Jiang, P. Cui, Q. Wang, Z. Wang, L. Wu and J. Liu, *Inorg. Chem. Front.*, 2020, **7**, 385–393.

4 M. Huang, L. Wang, K. Pei, W. You, X. Yu, Z. Wu and R. Che, *Small*, ,

DOI:10.1002/SMLL.202000158.

5 L. Wang, M. Huang, X. Yu, W. You, J. Zhang, X. Liu, M. Wang and R. Che, *Nano-Micro Lett.*, , DOI:10.1007/S40820-020-00488-0.

6 L. Wang, X. Yu, X. Li, J. Zhang, M. Wang and R. Che, *Chem. Eng. J.*, , DOI:10.1016/J.CEJ.2019.123099.

7 Y. Zhao, W. Wang, Q. Wang, H. Zhao, P. Li, J. Yan, G. Wang, W. Zhao, J. Yun, Z. Deng and Z. Zhang, *Carbon N. Y.*, 2021, **185**, 514–525.

8 M. Kong, X. Liu, Z. Jia, B. Wang, X. Wu and G. Wu, *J. Colloid Interface Sci.*, 2021, **604**, 39–51.

9 G. Song, K. Yang, L. Gai, Y. Li, Q. An, Z. Xiao and S. Zhai, *Compos. Part A Appl. Sci. Manuf.*, , DOI:10.1016/J.COMPOSITESA.2021.106584.

10 J. Tao, Z. Jiao, L. Xu, P. Yi, Z. Yao, F. Yang, C. Zhou, P. Chen, J. Zhou and Z. Li, *Carbon N. Y.*, 2021, **184**, 571–582.